Article

Particle Swam Optimization Based Fault Location and Restoration Approach in Microgrids

Wei-Tzer Huang [1,*], Kai-Chao Yao [1], Feng-Ying Wang [1], Chun-Chiang Ma [1], Hong-Ting Chen [1], Ping-Hsuan Hsieh [2]

[1] Department of Industrial Education and Technology, National Changhua University of Education, No. 2, Shida Rd., Changhua 500, Taiwan; kcyao@cc.ncue.edu.tw (K.-C.Y.); a047617333@yahoo.com.tw (F.-Y.W.); ma99002007@gmail.com (C.-C.M.); edchen1991@gmail.com (H.-T.C.)

[2] Department of Electrical Engineering, National Taiwan University of Science and Technology, No.43, Sec. 4, Keelung Rd., Da'an Dist., Taipei City 106, Taiwan; m10407104@gapps.ntust.edu.tw (P.-H.H.)

* Correspondence: vichuangl@cc.ncue.edu.tw (W.-T.H.); Tel.: +886-939-828-628 (W.-T.H.)

Abstract: This work aims to develop an integrated fault location and restoration approach for microgrids (MGs). This work contains two parts. Part I presents the fault location algorithm, and Part II shows the restoration algorithm. The proposed algorithms are implemented by particle swarm optimization (PSO). The fault location algorithm is based on network connection matrices, which are the modifications of bus-injection to branch-current and branch-current to bus-voltage (BCBV) matrices, to form the new system topology. The backward/forward sweep approach is used for the prefault power flow analysis. After the occurrence of fault, the voltage variation at each bus is calculated by using the Z_{bus} modification algorithm to modify Z_{bus}. Subsequently, the voltage error matrix is computed to search for the fault section by using PSO. After the allocation of the fault section, the multi-objective function is implemented by PSO for optimal restoration with its constraints. Finally, the IEEE 37-bus test system connected to distributed generations is utilized as the sample system for a series simulation and analysis. The outcomes demonstrated that the proposed optimal algorithm can effectively solve the fault location and restoration problem in MGs.

Keywords: Fault location; Service restoration; Particle swam optimization; Microgrid; Power flow; Short-circuit fault

1. Introduction

Microgrids (MGs) can be regarded as a set of load clusters, distributed generations (DGs), and energy storage systems [1-3]. In terms of the traditional power grid, MGs are the partial active networks in distribution systems. Therefore, MGs could be formed and owned in any possible type, such as utility and customer MGs. Utility MGs could be distribution substations, main transformers, full feeders, partial feeders, or distribution transformer-level MGs. However, regardless of their types, MGs are capable of operating in grid-tied and islanding modes through the point of common coupling, which is the connection point between the MGs and the main grid made by a static switch. Traditional passive distribution networks, which do not have DG interconnection, spend more than half an hour for fault detection, isolation, and restoration (FDIR). As a result of the high penetration of DGs in feeders to form active distribution networks, a large amount of data are available and are received by the feeder dispatch control center or distribution dispatch control center; consequently, the FDIR concept in distribution contingencies is different, in which the rigorous fault current calculation approaches are proposed by DGs[4-8]. Besides, the advanced information and communication techniques in FDIR are proposed to restore power to as many systems as possible and to reduce power restoration time after the occurrence of feeder faults in a radial-type feeder arrangement [9-11]. In the past few decades, the customers in rural distribution networks served by

many power companies have been experiencing long duration of power outages, especially those in upstream networks. In recent years, the possible solution for rapid and effective restoration is to operate these feeders as MGs because DGs that are composed of photovoltaics and wind power are interconnected into rural distribution feeders. Huijuan et. al [12] presented a case study to provide recommendations for utilities to evaluate the feasibility of MG operation as a potential solution to improve power supply reliability in rural feeders during a power outage. The key points of FDIR in MGs for outages attributed to overhead conductors or underground cables are fault location and restoration algorithms; therefore, IEEE Std C37.114 [13] and EPPRI [14] presented essential data and approaches for distribution fault location. Krishnathevar and Ngu [15] proposed the one-end impedance-based fault location method applied to distribution system; however, this method cannot be used for unbalanced three-phase systems. Brahma [16] also proposed an approach that uses synchronized voltage and current measurements at the interconnection of DG units in distribution systems to overcome the fault location errors caused by fault currents contributed by DGs. Wang et. al [17] proposed an effective ground fault location scheme using unsynchronized data for multi-terminal lines; this scheme does not require the data from each terminal to be synchronized. Yang et. al [18] presented a joint power restoration approach in active distribution networks that combines DG local restoration and switcher operation-based restoration to enhance self-healing; additionally, they formulated a stochastic mixed-integer linear program to maximize the served load presented in [19]. Wang et. al [20] proposed a decentralized outage detection algorithm that uses AMI meters to obtain the total number of customers and the total amount of lost load in the outage area. The black start capability for MGs is vital. Hence, Wang et. al [21] proposed a parallel restoration strategy that considers the characteristics of DGs for MG black start. These state-of-the-art studies presented power restoration approaches in modern active distribution networks and revealed that MGs are distinct from traditional passive radial-type networks. MGs provide feasible and reliable power restoration after an upstream system outage, such as transmission line, main transformer, and feeder failures. In the current work, an integrated fault location and restoration approach for MGs is proposed to effectively solve the FDIR problem in MGs. This paper is divided into six sections. Section 1 introduces the background and objective of this study. Section 2 describes the flow chart of the proposed approach. Section 3 explains the fault location algorithm and solution procedure. Section 4 presents the power restoration algorithm and solution procedure. Section 5 discusses the simulation results. Section 6 presents the conclusion.

2. Problem Description of Fault Location and Service Restoration in MGs

The fault location and restoration problem of MGs can be divided into two layers. The flow chart of the proposed approach is shown in Figure 1. The first priority is to establish the network topology by using bus connection matrices based on graph theory; the bus impedance matrix (Z_{Bus}) can be easily obtained by multiplying the bus-injection to branch-current (BIBC) and the branch-current to bus-voltage (BCBV) matrices [22,23] according to the system topology that changes during pre-fault and fault conditions.

The methods used for fault detection and isolation are summarized as follows:

(1) Impedance method
(2) High-frequency components and wavelet transform
(3) Artificial neural network
(4) Comparison measurement and simulation value
(5) Hybrid method

In general, the fault current contributed by the upstream main grid and DGs causes bus voltage variation, and it is used to determine the fault location in MGs. Brahma [16] used synchronized voltage and current measurements to detect the fault section for distribution systems with high DG penetration; however, how to effectively rebuild the Z_{Bus} after fault occurred is the key factor; unfortunately, lots of researches are weakly in this part, and the advantage of this paper is to effectively rebuild the Z_{Bus} corresponding to network topology under post-fault conduction. The concept of the proposed approach in this paper is based onthe impedance method, PSO, and the

Preprints (www.preprints.org) | NOT PEER-REVIEWED | Posted: 12 September 2019 doi:10.20944/preprints201909.0127.v1

synchronized voltage and current measurement technique proposed in [16]. It is distinct that a systematic and effective graph theory-based algorithm is proposed for fault location in MGs. Therefore, only a minor modification of the BIBC matrix built in the pre-fault stage is needed in the fault stage; and a new, fast, and effective Z_{Bus} is derived. This approach is applicable to unbalanced distribution networks and is distinct from the traditional Z_{Bus} modification method, which is used in three-phase balanced systems. Service restoration implemented by PSO algorithm follows fault detection and isolation and is aimed at a minimum operation number of switches and loss of electricity service.

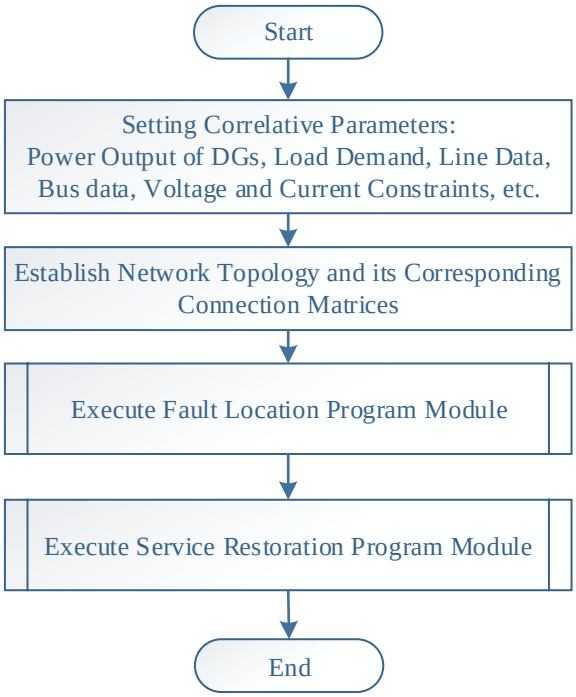

Figure 1. Proposed fault detection, isolation, and restoration of MGs.

3. Derivation of Fault Location Approach

The fault location approach proposed in this study is described in detail. The first step of the proposed method is to calculate the pre-fault and fault bus voltages. Therefore, a fast and systematic power flow method should be developed to avoid rebuilding Z_{Bus} due to the different network topologies before and after the occurrence of a fault. Consequently, graph theory is applied to develop the bus impedance matrix for the power flow solution and fault current calculation. Finally, the proposed voltage error matrix (VEM) and particle swarm optimization (PSO) are used to determine the fault location. The detailed theory of the proposed method is described here.

3.1. Graph Theory-based Power Flow Algorithm

For a convenient combination of Z_{Bus}, graph theory and backward/forward sweep algorithm are applied in power flow analysis. A systematic approach, graph theory, is use to build incidence matrices that correspond to network topologies. The proposed algorithm use the A incidence matrix, which is the element–bus incidence matrix; and the K matrix, which is the branch–path incidence matrix. The BIBC and BCBV matrices can be established according to the network topology based on these matrices. Furthermore, the BIBC and BCBV matrices are applied in the power flow algorithm. The solution procedure of the proposed power flow is described as follows.

Step 1: Establish A matrix. Derive K matrix using Equation (1). Build the BIBC matrix using Equation (2).

$$K=[A^{-1}]^t \quad (1)$$

Preprints (www.preprints.org) | NOT PEER-REVIEWED | Posted: 12 September 2019 doi:10.20944/preprints201909.0127.v1

$$[BIBC]=-K \tag{2}$$

Step 2: Transpose the BIBC matrix and add the primitive line impedance, which means total series impedance between two connection buses into the corresponding non-zero element position to derive the BCBV matrix.

Step 3: Build the bus impedance matrix using Equation (3) by multiplying the BIBC and BCBV matrices.

$$[Z_{Bus}]=[BIBC][BCBV] \tag{3}$$

Step 4: Calculate the equivalent bus injection current at each bus connected to the source or load using Equation (4).

$$I_i^k=(\frac{P_i+Q_i}{V_i^k})^* \tag{4}$$

Step 5: Compute the voltage derivation of each bus using Equation (5).

$$[\Delta V^k]=[Z_{Bus}][I^k] \tag{5}$$

Step 6: Using Equation (6) to update the bus voltage, where V_{no_load} is the no-load voltage at each bus, i.e. the bus voltage is assumed as 1.0 pu, that is,

$$[V^{k+1}]=[V_{no\_load}]-[\Delta V^k]. \tag{6}$$

Step 7: Check the convergence by Equation (7). If the Equation (7) is true, then it is not convergence; therefore, proceed to Step 4; otherwise, end the solution procedure. ε is the maximum toleration, that is,

$$max_i(\left|I_i^{k+1}\right|-\left|I_i^k\right|)>\varepsilon. \tag{7}$$

3.2. Fault Location Alogrithm Based on Z_{Bus}

The proposed fault location algorithm uses the bus voltage variation, which is caused by the fault current contributed by the upstream utility grid, and distributed energy resources to determine fault locations. A fast Z_{Bus} modified algorithm based on the BIBC and BCBV matrices is necessary for the rigid computation of the bus voltage variations before and after the occurrence of a fault. Therefore, Z_{Bus} can be built by using Equation (3) according to the pre-fault network topology. Z_{Bus} needs to be modified when a short-circuit fault occurs at bus *k*. We assume that the MGs are equipped with measuring devices placed at the output terminals of each DG unit. During fault conditions, the values of zero-sequence, positive-sequence, and negative-sequence voltages and currents are recorded by the measuring devices and can be used to obtain the zero-, positive-, and negative-sequence Thevenin impedances of the DGs [24], respectively. The phase frame impedance of the DGs are calculated by using Equation (8), where $a=e^{j2\pi/3}$. The derived Thevenin impedances of all DGs are added as branches from the connected buses to the reference bus. Consequently, Z_{Bus} can be modified according to the minor change of the BIBC and BCBV matrices.

$$Z_{abc}=\begin{pmatrix} Z_{Sa} & Z_{Sab} & Z_{Sac} \\ Z_{Sba} & Z_{Sb} & Z_{Sbc} \\ Z_{Sca} & Z_{Scb} & Z_{Sc} \end{pmatrix}=\frac{1}{3}\begin{pmatrix} 1 & 1 & 1 \\ 1 & a & a^2 \\ 1 & a^2 & a \end{pmatrix}\begin{pmatrix} Z_S^{(0)} & 0 & 0 \\ 0 & Z_S^{(1)} & 0 \\ 0 & 0 & Z_S^{(2)} \end{pmatrix}\begin{pmatrix} 1 & 1 & 1 \\ 1 & a^2 & a \\ 1 & a & a^2 \end{pmatrix} \tag{8}$$

While a three-phase short-circuit fault occurs at bus *j*, the bus voltage can be expressed as the pre-fault voltage plus the voltage deviation caused by the fault current by Equation (9). The voltage at faulted bus *j* can be obtained by Equation (10) and can also be derived by multiplying the fault current by the fault impedance as shown in Equation (11).

Preprints (www.preprints.org) | NOT PEER-REVIEWED | Posted: 12 September 2019 doi:10.20944/preprints201909.0127.v1

$$\begin{bmatrix} V_1^{abc}(F) \\ \vdots \\ V_j^{abc}(F) \\ \vdots \\ V_n^{abc}(F) \end{bmatrix} = \begin{bmatrix} V_1^{abc}(0) \\ \vdots \\ V_j^{abc}(0) \\ \vdots \\ V_n^{abc}(0) \end{bmatrix} + \begin{bmatrix} Z_{11}^{abc} & \cdots & Z_{1j}^{abc} & \cdots & Z_{1n}^{abc} \\ \vdots & \vdots & \vdots & \vdots & \vdots \\ Z_{j1}^{abc} & \cdots & Z_{jj}^{abc} & \cdots & Z_{jn}^{abc} \\ \vdots & \vdots & \vdots & \vdots & \vdots \\ Z_{n1}^{abc} & \cdots & Z_{nj}^{abc} & \cdots & Z_{nn}^{abc} \end{bmatrix} \begin{bmatrix} 0 \\ \vdots \\ -I_j^{abc}(F) \\ \vdots \\ 0 \end{bmatrix} \quad (9)$$

$$V_j^{abc}(F) = V_j^{abc}(0) - Z_{jj}^{abc} I_j^{abc}(F) \quad (10)$$

$$V_j^{abc}(F) = Z_f^{abc} I_j^{abc}(F) \quad (11)$$

Therefore, the fault current can be obtained from Equations (10) and (11), as shown in Equation (12), for the three-phase bolted fault. $Z_f^{abc}=0$, and $V_j^{abc}(F)=0$.

$$I_j^{abc}(F) = \frac{V_j^{abc}(0)}{Z_{jj}^{abc} + Z_f^{abc}} \quad (12)$$

where,

$V_j^{abc}(0)$ is the pre-fault three-phase voltage at bus *j*.

$I_j^{abc}(F)$ is the fault three-phase current from bus *j* to the ground.

Z_{jj}^{abc} is the equivalent three-phase impedance from bus *j* and can be obtained from Z_{Bus}.

Z_f^{abc} is the three-phase fault impedance.

Using Equation (12), the bus voltage derivation at bus *i* due to a fault at bus *j* is expressed as Equation (13).

$$\Delta V_{i-j}^{abc} = Z_{bus}(i,j) \times I_j^{abc}(F) \quad (13)$$

The three-phase bus voltage derivation at all DG buses for the assumed fault location can be calculated by Equation (13). The first step of the proposed algorithm is to calculate the voltage error at each bus, as shown in Equation (14). The voltage error at bus *j* is expressed as the norm of the difference between the voltage derivation and the value of the measured voltage. The voltage derivation ($\Delta V_{S(i)-f(j)}^{abc}$) at bus *j* is caused by the fault current contributed by source bus *i*, which represents the upstream utility grid or DG. The value of the measured voltage ($\Delta V_{S(i)-meas.}^{abc}$) can be obtained by the synchronized voltage and current measurement device with millisecond level response time installed in each fault current contributed source from the energy management system of the MG, and m in Equation (14) represents the number of fault current sources. For an *n*-bus MG, the VEM can be established, as shown in Equation (15). The smallest value of the element in the VEM denotes the short-circuit faulted bus. It is noteworthy that the fault current is about ten times of the normal load current generally; besides, the fault current contributed by DG is two times of the rated output current limited by inverter of photovoltaic. Therefore, the measurement device is able to distinguish the fault current and normal current contributed by load and DG, and then the bus voltage deviation could be distinguished from caused by fault current or normal current.

$$ve_j = \sum_{i=1}^{m} \sqrt{\left(\Delta V_{S(i)-f(j)}^{a} - \Delta V_{S(i)-meas.}^{a}\right)^2 + \left(\Delta V_{S(i)-f(j)}^{b} - \Delta V_{S(i)-meas.}^{b}\right)^2 + \left(\Delta V_{S(i)-f(j)}^{c} - \Delta V_{S(i)-meas.}^{c}\right)^2} \quad (14)$$

$$\mathbf{VEM} = \left[ve_1 \quad \cdots \quad ve_j \quad \cdots \quad ve_n \right], \; Bus \text{ number} = 1,...,n \quad (15)$$

Preprints (www.preprints.org) | NOT PEER-REVIEWED | Posted: 12 September 2019 doi:10.20944/preprints201909.0127.v1

3.3. Solution Procedure of the Proposed Fault Location Algorithm

Short-circuit fault may occur at the bus or in the line segment. Thus, Z_{Bus} can be modified in two conditions. If the fault occurs at the bus, then Z_{Bus} don't need to be modified. Otherwise, if the fault occurs in the line segment, a negative impedance of the line segment should be added to remove the original line segment. Then, a virtual bus that is assumed in the middle of the line segment, as well as two elements, should be added, with one element added as a new branch from the existing bus to the virtual bus and with the other element added as a new link from the virtual bus to the other existing bus, the procedure is shown in Figure 2. Therefore, the dimension of the BIBC matrix becomes $(n+1)\times(n+1)$, and the new Z_{Bus} can be derived by using Equation (3). The fault point is assumed at the virtual bus. In this study, PSO [25,26] is used to search for the faulted bus, and the assumed faulted bus is modeled as a particle whose objective function is shown in Equation (14). The proposed fault location approach of the MG is shown in Figure 3.

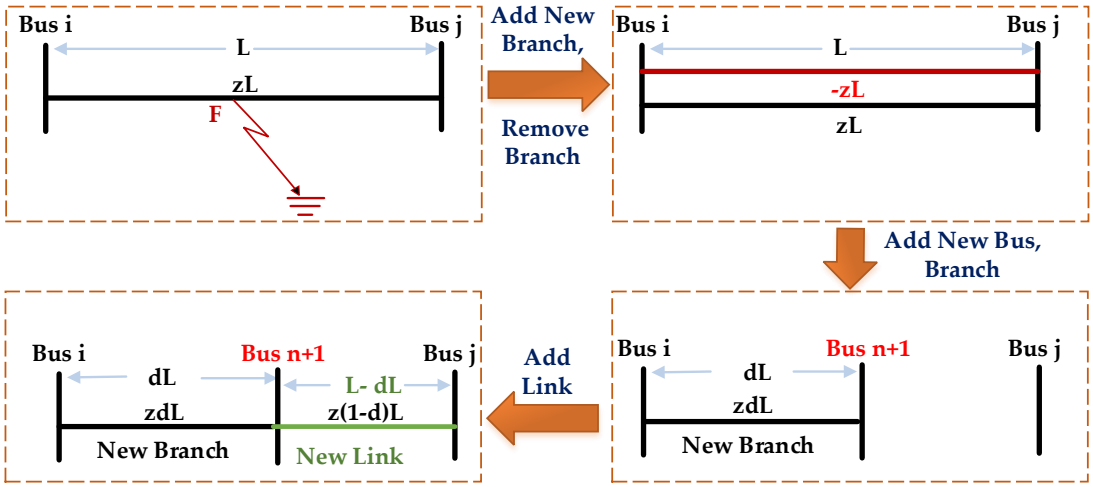

Figure 2. Z_{Bus} modification procedure for adding a virtual bus.

Preprints (www.preprints.org) | NOT PEER-REVIEWED | Posted: 12 September 2019 doi:10.20944/preprints201909.0127.v1

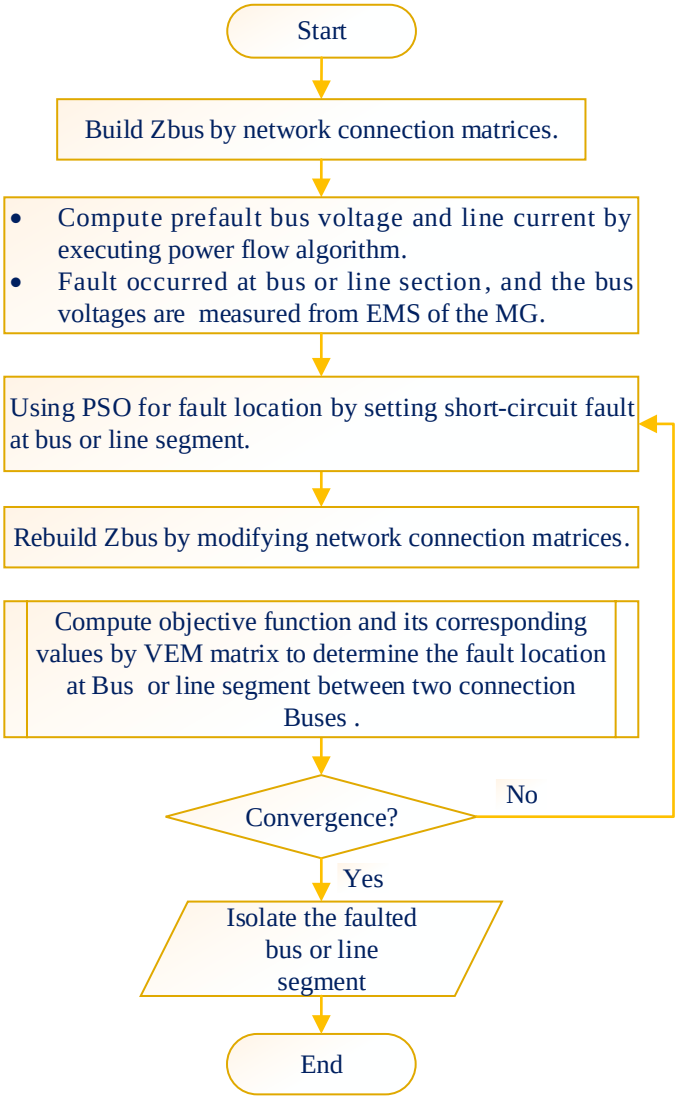

Figure 3. Proposed fault location approach of the MG.

4. Proposed Service Restoration Approach

MGs are capable of grid-tied and islanding operations integrated with DGs and loads. Therefore, the electricity service restoration can be divided into two operation modes. Regardless of the operation mode, service restoration is aimed at reducing the out-of-service un-faulted zone and then minimizing its effect. Consequently, the service restoration problem can be described as the minimization of a multi-objective non-linear problem that is composed of the loss of load service, the number of switch operations, and power loss, as shown in Equation (16).

$$\min\ F = w_1 \times \frac{P_{loss-service} - P_{loss-service}^{\min}}{P_{loss-service}^{\max} - P_{loss-service}^{\min}} + w_2 \times \frac{n_{ops} - n_{ops}^{\min}}{n_{ops}^{\max} - n_{ops}^{\min}} + w_3 \times \frac{P_{loss} - P_{loss}^{\min}}{P_{loss}^{\max} - P_{loss}^{\min}} \quad (16)$$

subject to

$$w_1 + w_2 + w_3 = 1, \quad (17)$$

$$I \le I^{\max}, \quad (18)$$

$$V^{\min} \le V \le V^{\max}, \quad (19)$$

Preprints (www.preprints.org) | NOT PEER-REVIEWED | Posted: 12 September 2019 doi:10.20944/preprints201909.0127.v1

where $P_{loss-service}$ denotes the loss of load service; n_{ops} represents the number of switch operations; P_{loss} denotes the system power loss; w_i denotes a weighting factor that can be adjusted for the requirement; I^{max} is the ampere capacity of the conductor; and V^{min} and V^{max} represent the lower and upper limits of bus voltage, respectively. The related parameters of the objective function and constraints are set to w_1=0.2, w_2=0.1, and w_3=0.7. Furthermore, the lower and upper limits of the bus voltage are 0.95–1.05 pu, and the ampere capacity is 300 A.

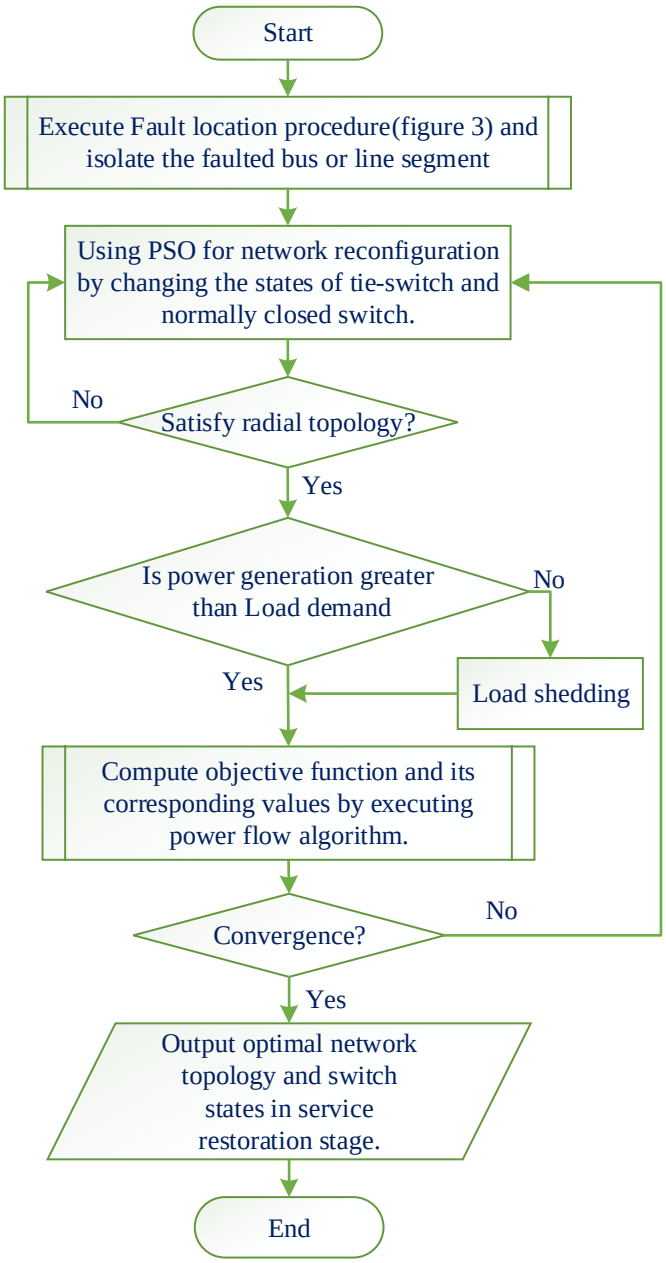

Figure 4. Proposed service restoration algorithm of the MG.

By applying the PSO algorithm to solve the proposed service restoration approach, the A matrix is built according to the switch status and must be transferred to the PSO algorithm to obtain the corresponding network topology. The power flow algorithm is used to compute the specified network topology, and the value of the proposed function of each particle is obtained. PSO, which is combined of the *pbest* and *gbest*, allows a particle to fast and correct adjust, thereby resulting in rapid convergence using Equations (20)-(24).

Preprints (www.preprints.org) | NOT PEER-REVIEWED | Posted: 12 September 2019 doi:10.20944/preprints201909.0127.v1

$$V_n^{k+1} = V_n^k + c_1 \times rand_1 \times (pbest_n^k - s_n^k) \tag{20}$$

$$V_n^{k+1} = V_n^k + c_2 \times rand_2 \times (gbest^k - s_n^k) \tag{21}$$

$$V_n^{k+1} = w \times V_n^k + c_1 \times rand_1 \times (pbest_n^k - s_n^k) + c_2 \times rand_2 \times (gbest^k - s_n^k) \tag{22}$$

$$s_n^{k+1} = s_n^k + v_n^{k+1} \tag{23}$$

$$w = w_{\max} - (w_{\max} - w_{\min}) \times \frac{k}{k_{\max}} \tag{24}$$

where V_n^k denotes the velocity of the n^{th} particle at the k^{th} iteration, s_n^k represents the k^{th} position of the n^{th} particle, the learning factors are represented as c_1 and c_2, the random numbers of $rand_1$ and $rand_2$ are between 0 and 1, $pbest_n^k$ denotes the best value of the n^{th} particle at the k^{th} iteration, and $gbest^k$ denotes the global best value at the k^{th} iteration. w, w_{max}, and w_{min} are acceleration coefficients, maximum weighting values, and minimum weighting values, respectively; n denotes the particle number; k_{max} denotes the maximum iteration. In this study, the related parameters of PSO are set to $n = 500$, $w_{max} = 0.9$, $w_{min} = 0.2$, $c_1 = 2$, and $c_2 = 2$; the maximum iteration number is 200. The detailed solution procedure of the service restoration is illustrated in Figure 4.

5. Numerical Results and Discussions

The MG modified from the IEEE 37-bus test system is utilized as a sample system to verify the effectiveness of the proposed method. The original IEEE 37-bus test system is a traditional distribution network whose line and bus data are shown in [27]. The system is a three-phase unbalanced passive network that is only connected with loads. The simulation results under grid-tied and islanding operation modes are discussed in the following sections.

5.1. Description of the Sample System and Simulation Scenarios

The MG sample system is modified on the basis of the IEEE 37-bus test system (Figure 5). Five new tie lines and switches are added as follows. S36 is installed between buses 701 and 722. S37 is installed between buses 735 and 741. S38 is installed between buses 727 and 732. S39 is installed between buses 725 and 731. S40 is installed between buses 712 and 740. In addition, the DGs are connected at buses 724, 731, and 740. The parameters of the tie switches and lines are shown in Table 1. The power outputs of the DG at buses 724, 731, and 740 are 595, 460, and 150 kW, respectively.

The simulation scenarios are presented in Table 2, and the scenarios are explained as follows.

- ✓ Scenario 1: A single-point fault in the line segment is assumed between buses 702 and 703. This fault is used to simulate a situation in which most of the downstream areas of the MG are affected due to the fault that occurred in the upstream of the MG.
- ✓ Scenario 2: A double-point fault in a line segment is assumed: one point is between buses 702 and 703, and the other point is between buses 727 and 703. This fault is used to simulate multiple power outages in downstream areas. Multiple tie switches and lines must be operated at the same time for service restoration.
- ✓ Scenario 3: A triple-point fault in the line segment is assumed. The multiple fault points are between buses 702 and 703, buses 727 and 703, and buses 710 and 734. This fault is used to simulate power generation less than the load demand in the downstream islanded area. Load shedding is required for this situation.

In this study, a co-analysis and simulation platform is established (Figure 6). The sample system is built in OpenDSS [28] and MATLAB: the value of the measured voltage of the sample system is obtained by OpenDSS, and the proposed fault location, service restoration, and power flow algorithms are coded in MATLAB.

Preprints (www.preprints.org) | NOT PEER-REVIEWED | Posted: 12 September 2019 doi:10.20944/preprints201909.0127.v1

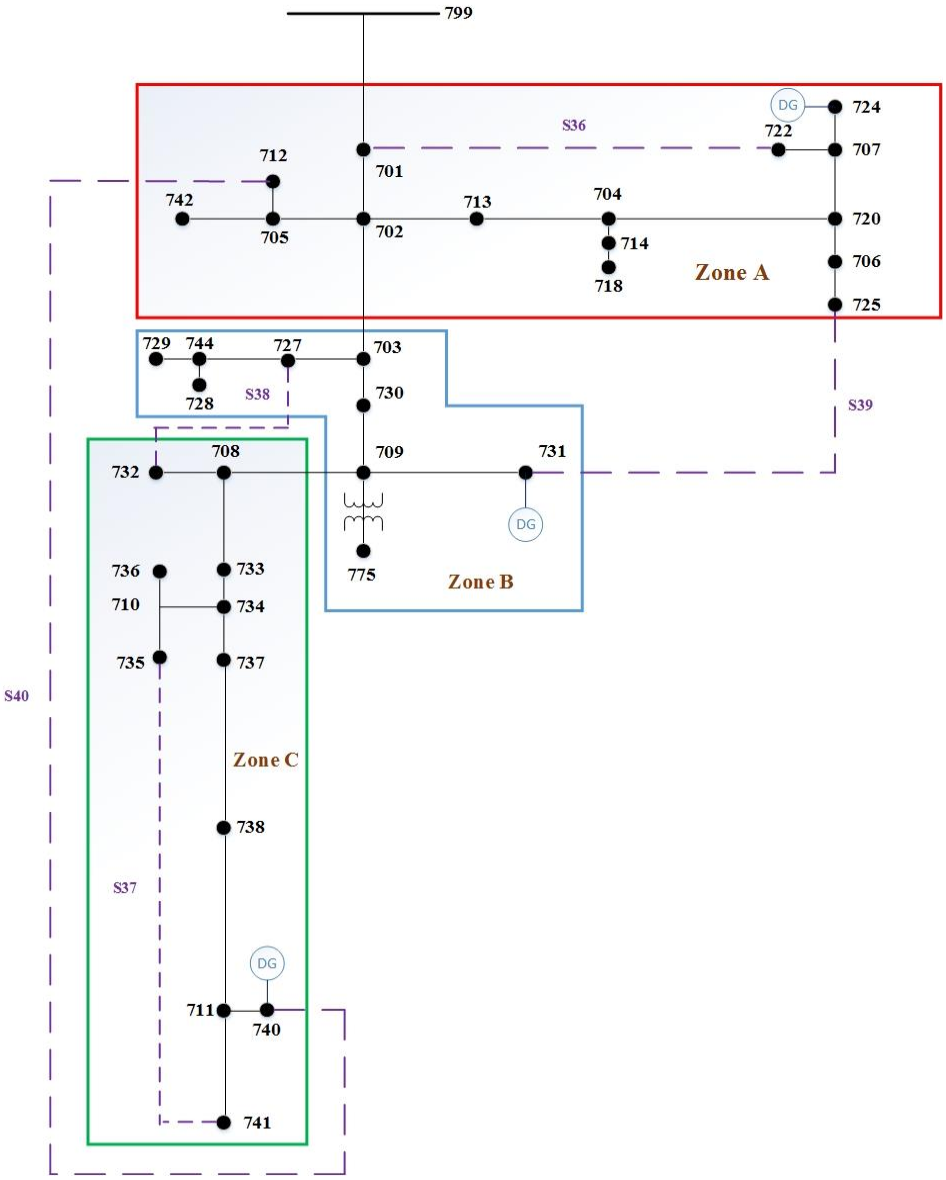

Figure 5. Single-line diagram of the sample system.

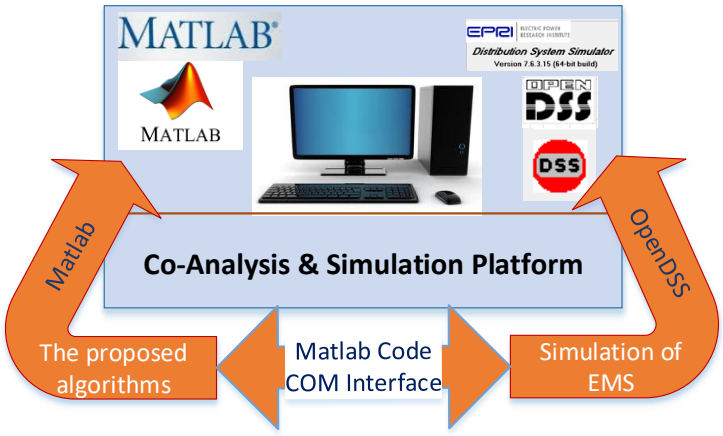

Figure 6. Co-analysis and simulation platform.

Preprints (www.preprints.org) | NOT PEER-REVIEWED | Posted: 12 September 2019 doi:10.20944/preprints201909.0127.v1

Table 1. Parameters of tie switches and lines.

Switch No.	From Bus	To Bus	Length(m)	Voltage	Phase
S36	701	722	91.44	4.8 kV	ABC
S37	741	735	152.40	4.8 kV	ABC
S38	727	732	60.96	4.8 kV	ABC
S39	725	731	243.84	4.8 kV	ABC
S40	712	740	457.20	4.8 kV	ABC

Table 2. Fault point assumption of each scenario.

Scenario	Fault Type	Fault point between two buses
Scenario 1	Three-phase short-circuit fault	702-703
Scenario 2	Three-phase short-circuit fault	702-703, 727-703
Scenario 3	Three-phase short-circuit fault	702-703, 727-703, 710-734

5.2. Grid-Tied Operation

Table 3 illustrates the simulation results of the sample system and the scenarios assumed in Section 5.1 according to the proposed fault location and service restoration algorithms in this study. The network topologies that correspond to each scenario are illustrated in Figures 7 (a), (b), and (c).

In Scenario 1, a three-phase bolted short-circuit fault occurs in line segment 702–703, which is between buses 702 and 703. Fault is detected in line segment 702–703 according to the minimal value of the voltage deviation in the VEM using the proposed fault location algorithm (Equation (15)). The proposed service restoration algorithm is used to restore power supply to the un-faulted area. Therefore, according to the convergence of the numerical results of the objective function and the related constraints (Equations 16–18), the switch between line segment 708–709 is opened, and two tie switches (i.e., S39 and S40) are closed to form the network topology (Figure 7(a)). The service restoration percentage is 100% because of the fault that occurs in the line segment, and the operations of the tie switches successfully restore electricity service. The power loss is 62.47 kW in this radial type topology, and all the line currents and bus voltages satisfy their limits.

In Scenario 2, the fault type is the same as that in Scenario 1, that is, a double fault occurring in line segments 702–703 and 727–703. These two fault points are detected by two minimal values in the VEM. The switch between line segment 708–733 is opened, and three tie switches, namely, S38, S39, and S40, are closed to form the network topology, as shown in Figure 7(b). Similar to Scenario 1, the service restoration percentage is 100%, the power loss is 61.47 kW, all the line currents are less than 300 A, and the bus voltages are within 0.95–1.05 pu. The simulation results illustrate that the combined fault location and restoration approach is capable of dealing with double-point fault conditions.

In Scenario 3, a triple fault occurs in line segments 702–703, 727–703, and 710–734. These multiple fault points are detected by three minimal values in the VEM. The switch between line segment 708–733 is opened, and four tie switches, namely, S37, S38, S39, and S40, are closed to form the network topology, as shown in Figure 7(c). Similarly, the service restoration percentage is 100%, the power loss is 60.46 kW, and all the line currents and the bus voltages do not violate these limits. The outcomes demonstrate that the proposed approach is capable of multiple-point fault detection, isolation, and restoration.

(a) (b) (c)

Preprints (www.preprints.org) | NOT PEER-REVIEWED | Posted: 12 September 2019 doi:10.20944/preprints201909.0127.v1

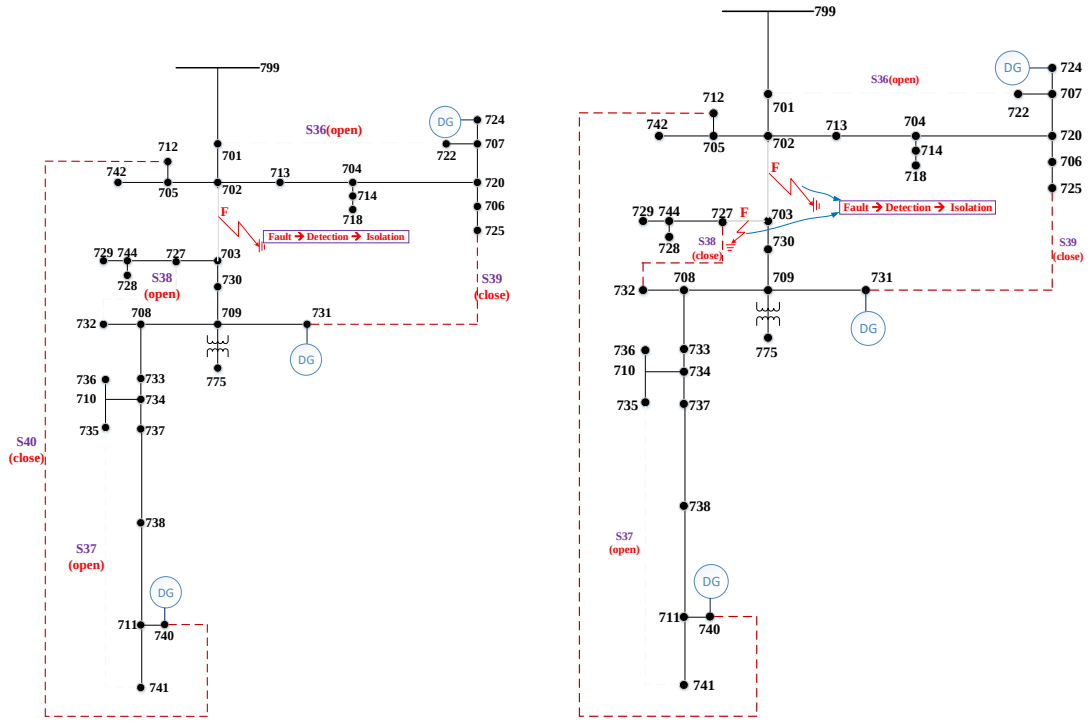

(a) Scenario 1

(b) Scenario 2

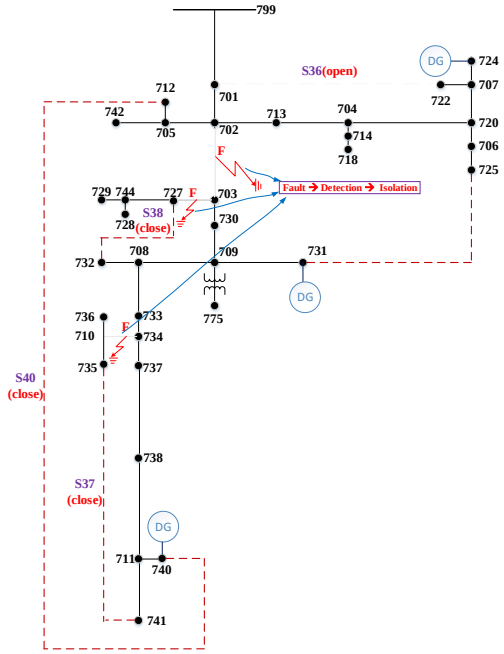

(c) Scenario 3

Figure 7. Network topologies of the Sample System after service restoration.

Table 3. Simulation Results under grid-tied operation mode.

Scenario	Fault Location	Switch			Restoration (%)	Power Loss	Radial Type
		Open	Close	Operation Number			
1	702-703	S(708-709)	**S39 S40,**	3	100%	62.67 kW	Yes
2	702-703	S(708-733)	**S38**	4	100%	61.47 kW	Yes

Preprints (www.preprints.org) | NOT PEER-REVIEWED | Posted: 12 September 2019 doi:10.20944/preprints201909.0127.v1

3	727-703 702-703 727-703 710-734	S(708-733)	**S39** **S40**, **S37** **S38** **S39** **S40**,	5	100%	60.46 kW	Yes

298 *5.3. Islanding Operation*

299 The single-line diagram of the sample system under islanding operation mode is shown in
300 Figure 8. In the islanding operation mode, the available power output of the DGs plays a key role to
301 ensure a stable system operation because no utility power grid acts as a swing bus. System frequency
302 and voltage magnitude are kept constant in accordance with the power balance principle.
303 Consequently, if the power generation of DGs is greater than the load demand, then the optimal
304 dispatch method automatically adjusts the power output to meet the power balance requirement.
305 Otherwise, the load shedding strategy should be used to maintain power balance. The loads are
306 classified into critical and common loads. The symbol of critical load is expressed as "O," and the
307 symbol of non-critical load is represented as "☆" (Figure 8). The first priority of load shedding is non-
308 critical load and then critical load. The simulation results of the sample system and the assumed
309 scenarios are listed in Table 4. In Scenario 1, the fault is detected in line segment 702–703 according
310 to the minimal value of voltage deviation in the VEM. The tie switch S39 is closed to form a network
311 topology (Figure 8). The service restoration percentage is 83.61% because the power output of the
312 DGs is less than the load demand. Load shedding is required to keep the power balance. In addition,
313 the power loss is 22.27 kW, and all the line currents and bus voltages satisfy their limits. In Scenario
314 2, these two fault points are detected by two minimal values in the VEM. Then, two tie switches,
315 namely, S38 and S39, are closed to form the network topology (Figure 8). The service restoration
316 percentage is 83.61%, the power loss is 22.41 kW, all the line currents are less than 300 A, and the bus
317 voltages are within 0.95–1.05 pu. In Scenario 3, the multiple-point fault is detected by three minimal
318 values in the VEM. Three tie switches, namely, S37, S38, and S39, are closed to form the network
319 topology. Similarly, the service restoration percentage is 83.61%, the power loss is 22.4 kW, and all
320 the line currents and the bus voltages do not violate the limits.

Preprints (www.preprints.org) | NOT PEER-REVIEWED | Posted: 12 September 2019 doi:10.20944/preprints201909.0127.v1

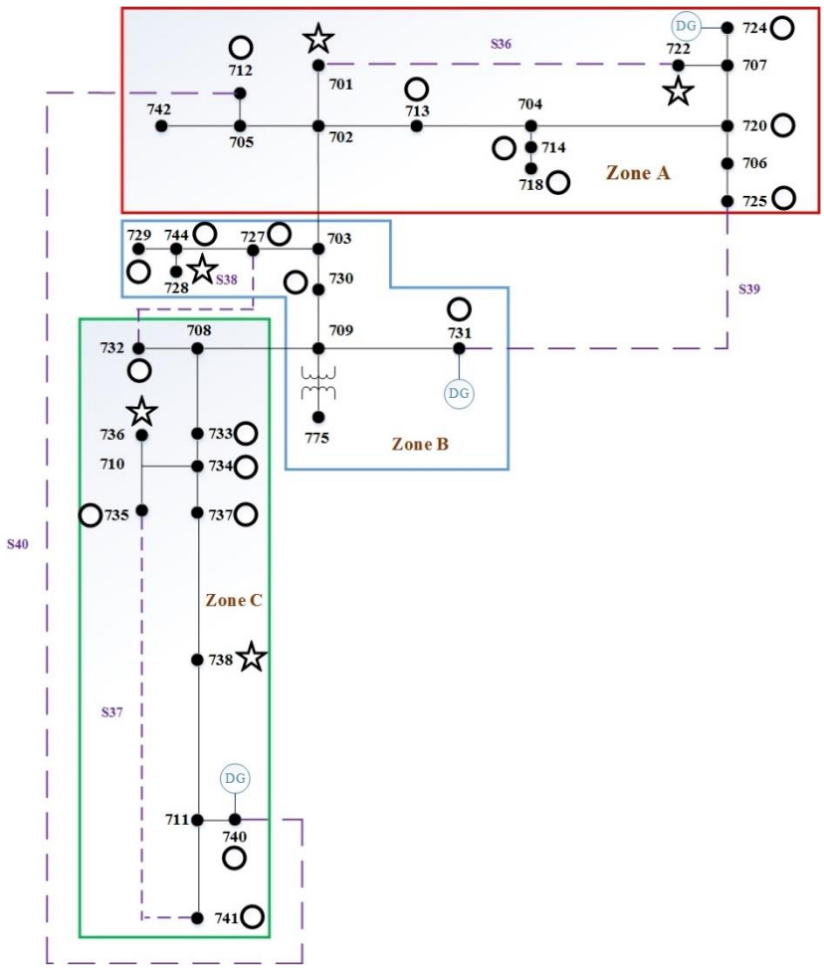

Figure 8. Single-line diagram of the sample system under islanding operation mode.

Table 4. Simulation Results under islanding operation mode.

Scenario	Fault Location	Switch			Load Shedding Bus	Restoration (%)	Power Loss	Radial Type
		Open	Close	Operation Number				
1	702-703	-	**S39**	1	701 722	83.61%	22.27 kW	Yes
2	702-703 727-703	-	**S38** **S39**	2	728 735	83.61%	22.41 kW	Yes
3	702-703 727-703 710-734	-	**S37** **S38** **S39**	3	736 737 738	83.61%	22.40 kW	Yes

6. Conclusion

In this study, a fault location and service restoration algorithm is developed and integrated for three-phase short circuit fault detection, isolation, and restoration in MGs. The proposed approach is based on a fast computing algorithm and the measured data from the EMS of MGs. Therefore, graph theory is used to establish BIBC and BCBV matrices for the corresponding network topology. The bus impedance matrix is effective and easy to build and modify for pre-fault and post-fault analyses without the need for the time-consuming rebuilding of a bus impedance matrix due to topology changes. Consequently, the bus impedance matrix is convenient to use in pre-fault power flow analysis and calculation of post-fault bus voltage change caused by the fault current contributed by

the upstream power gird and DGs. The multi-objective function, which is composed of load shedding, switch operations, and power loss with voltage drop and ampere capacity constraints, is proposed for service restoration. These algorithms are implemented by PSO for fault location and optimal service restoration. The MG modified from IEEE 37-bus is used as the sample system to demonstrate the feasibility of the proposed approach. The proposed approach is coded using Matlab and executed on a Windows 10 Intel® Core™ i5-7200U CPU @2.5 GHz personal computer, and the average operational time of IEEE 37-bus is around 122 sec. The numerical results illustrate maximal service restoration percentage with minimum switch operations and power loss under both operating modes. The outcomes show that the proposed approach is capable of detecting, isolating, and restoring three-phase short-circuit faults under the grid-tied and islanding operating modes of MGs.

Author Contributions: The original idea of the proposed algorithm for fault location and service restoration in MGs was done by Wei-Tzer Huang and Kai-Chao Yao. The author Feng-Ying Wang checked the simulation results and corrected the outcomes. The simulation scenarios and results were checked by Chun-Chiang Ma. The service restoration algorithm was coded by Hong-Ting Chen , and the fault location algorithm was coded by Ping-Hsuan Hsieh.

Acknowledgments: The authors are grateful for financial support from the Ministry of Science and Technology, Taiwan, under Grant MOST 107-3113-E-042A-001-CC2.

Conflicts of Interest: The authors declare no conflict of interest.

References

1. Lasseter, R. H. MicroGrids. IEEE Power and Energy Magazine **2007,** 5, 4, 78-94.
2. Nigim, Khaled A.; Lee, W. J. Micro Grid Integration Opportunities and Challenges. IEEE Power Engineering Society General Meeting **2007**, 1-6.
3. Lasseter, R. H.; Paigi, P.: Microgrid. A Conceptual Solution. IEEE Power Electronics Specialists Conference **2004**, 6, 4285-4290.
4. Xu, G.; Wu, S.; Tan, Y. Island Partition of Distribution System with Distributed Generators Considering Protection of Vulnerable Nodes. *Appl. Sci.* **2017**, *7*, 1057.
5. Orozco-Henao, C.; Suman Bretas, A.; Marín-Quintero, J.; Herrera-Orozco, A.; Pulgarín-Rivera, J.D.; Velez, J.C. Adaptive Impedance-Based Fault Location Algorithm for Active Distribution Networks. *Appl. Sci.* **2018**, *8*, 1563.
6. Zayandehroodi, H.; Mohamed, A.; Shareef, H., et al. Determining exact fault location in a distribution network in presence of DGs using RBF neural networks. IEEE Int. Conf. on Information Reuse and Integration (IRI) **2011**, 3–5.
7. Hany F. H.; Youssef, T.; Cintuglu, M. H.; Mohammed, O. A. Multi-Agent-Based Technique for Fault Location, Isolation, and Service Restoration. IEEE Transactions on Industry Applications **2017**,53, 3, 1841-1851.
8. Nordman, M.; Lehtonen, M. An agent concept for managing electrical distribution networks. IEEE Trans. Power Del. **2005**, 20, 2, 696–703.
9. Shahid, M. U.; Khan, M. M.; Hashmi, K.; Habib, S.; Jiang, H.; Tang, H. A Control Methodology for Load Sharing System Restoration in Islanded DC Micro Grid with Faulty Communication Links. *Electronics* **2018**, *7*, 90.
10. Zhao, Z.; Ooi, B. T. Feasibility of fast restoration of power systems by micro-grids. IET Generation, Transmission & Distribution **2017**, 12, (1), 126–132.
11. Le, D.P.; Bui, D.M.; Ngo, C.C.; Le, A.M.T. FLISR Approach for Smart Distribution Networks Using E-Terra Software—A Case Study. *Energies* **2018**, *11*, 3333.
12. Li, H.; Singhvi, V.; Maitra, A.; Rajagopalan S.; Enayati, B.; Santoso, S.; Patterson, R. National grid microgrid feasibility evaluation: Case study of a rural distribution feeder. IEEE PES General Meeting Conference & Exposition **2014**, 1–5.
13. IEEE Std C37.114. IEEE Guide for Determining Fault Location on AC Transmission and Distribution Lines. **2005**, 1-36.
14. EPPRI. Distribution Fault Location: -2004 Field Data and Analysis. Palo Alto, CA, **2006**.
15. Krishnathevar, R.; Ngu, E. E. Generalized Impedance-Based Fault Location for Distribution Systems. IEEE

Transactions on Power Delivery **2012**, 27, 1, 449–451.

16. Brahma, S. M. Fault Location in Power Distribution System with Penetration of Distributed Generation. IEEE Transactions on Power Delivery **2011**, 26, 3, 1545-1553.
17. Wang, D.; Ning, Y.; Zhang, C. An Effective Ground Fault Location Scheme Using Unsynchronized Data for Multi-Terminal Lines. *Energies* **2018**, *11*, 2957.
18. Yang, Q.; Jiang, L.; Ehsan, A.; Gao, Y.; Guo, S. Robust Power Supply Restoration for Self-Healing Active Distribution Networks Considering the Availability of Distributed Generation. *Energies* **2018**, *11*, 210.
19. Arif, A.; Wang, Z. Networked microgrid for service restoration in resilient distribution systems. IET Generation, Transmission & Distribution **2017**, 11, 14, 3612–3619.
20. Wang, Z.; Wang, J. Service restoration based on AMI and networked MGs under extreme weather events. IET Generation, Transmission & Distribution **2017**, 11, 2, 401–408.
21. Wang, J.; Mu, L.; Zhang, F.; Zhang, X. A Parallel Restoration for Black Start of Microgrids Considering Characteristics of Distributed Generations. *Energies* **2018**, *11*, 1.
22. Chen, T.H.; Yang, N. C. Three-phase power-flow by direct ZBR method for unbalanced radial distribution systems. *IET Generation, Transmission & Distribution* **2009**, *3*, 903-910.
23. Teng, J. H. A network-topology based three: phase load flow for distribution systems. *Proceedings of National Science Council ROC (A)* **2000,** *24*, 259-264.
24. Barker, P.; Mello, R. W. Determining the impact of distributed generation on power systems: Part 1—Radial power systems. *IEEE Power Eng. Soc. Summer Power Meeting* **2000**, 1645–1658.
25. Kennedy, J.; Eberhart, R. C. Particle swarm optimization. *IEEE Int. Conf. on Neural Networks* **1995**, 4, 1942-1948.
26. Eberhart, R. C.; Kennedy, J. A new optimizer using particle swarm theory. *IEEE Int. Symposium on Micro Machine and Human Science* **1995**, 39-43.
27. Distribution Test Feeders. http://ewh.ieee.org/soc/pes/dsacom/testfeeders/index.html (accessed on 5/1/2019).
28. Dugan, R. C.; McDermott, T. E. An Open Source Platform for Collaborating on Smart Grid Research. IEEE PES Gen. Meeting **2011**, 1 –7.